9^{th} *International Conference of Modeling, Optimization and Simulation - MOSIM'12*
June 6-8, 2012 - Bordeaux - France
"Performance, interoperability and safety for sustainable development"

PRACTICAL DESIGN OF MINIMAL ENERGY CONTROLS FOR AN ELECTRIC BICYCLE

D. GROSSOLEIL, D.MEIZEL

XLIM, UMR CNRS
Limoges University / ENSIL
16, rue Atlantis
87068 Limoges Cedex - France
grossoleil@ensil.unilim.fr, dominique.meizel@xlim.fr

ABSTRACT: *This communication presents the validation of a methodology to compute good approximations of minimal energy controllers under constraint of average speed. The application is an electric bicycle travelling along a given 3D path. The proposed method consists to 1) intelligently sample the research space then 2) apply A* (Astar) optimal pathfinding algorithm with an efficient heuristic. The results of this method are compared to the exact solution computed by continuous optimal control theory of an academic but relevant problem stated in an analytical smooth form. The approximate method provides results similar to the exact one with a significantly shorter computation time. The advantage of the A* algorithm is that it deals with unsmooth functions, inequality constraints, and long travels. This study is a milestone in a more global study about hybridization of human energy.*

KEYWORDS: *Optimal control, electric bicycle, A* algorithm, heuristics, performance evaluation.*

1 INTRODUCTION

Using (electric) bicycles for short travels (less than 20km/day) is spreading up in large agglomerations, often in complement with mass public transportations. It is relevant for two reasons. The former is a societal one: for a given travel demand, it decreases the emissions of polluting and greenhouse effect gases together while lowering traffic congestion. The latter is an individual one: the body of the transported person takes an active part to the travel which gives, for active people with sedentary jobs, the opportunity to have a reasonable physical training which is surely good for individual health. For small travels in flat cities, the usual bicycle is undoubtedly the healthier and minimal energy solution. For long or hilly travels, the electric bicycle is a good compromise between comfort and low energy transportation.
Timmermans et al. (2009) report in an objective benchmark that torque and energy consumption performances are very variable (from 4.8 Wh/km to 16.7 Wh/km for energy consumption). Only a few models are ranked fully satisfying.
Concerning constraints, numerous European countries regulations impose upper bounds for both the mechanical power of the electric motor (< 250W) and the speed ($<$25km/h). Within this legal framework, electric bicycle manufacturers have sufficient degrees of freedom to develop good controllers.

The electric bicycle is obviously a hybrid (human & electric) powered vehicle. Numerous studies deal with fuel consumption minimization on hybrid thermal/electric vehicle. An electric motor supplied by a battery constitutes a reversible embedded source of power. The energy has to be split optimally between the engine and the electric machine to minimize fuel consumption. Off line optimal controls are usually designed with a power demand specified by a priori known velocity and altitude profiles. Lin et al. (2003) compute the optimal power split of a hybrid electric truck with a dynamic programming method. This method samples the command and the state space. Such method implies heavy computation. Delprat et al. (2004) and Kim et al. (2011) use a method based on classical optimal control theory to build an optimal offline control applied to a hybrid car.
The present study is a part of a global one concerning the hybridization of human and electric energies that satisfies comfort or physical training prescription while optimizing the autonomy and availability of the device. Nevertheless, because optimal control is the relevant theory to deal with constrained problems of optimal autonomy, we propose here to first consider a limit case without human power. It gives an easier framework to validate a practical computation of a minimal energy control.
A realistic usage imposes a lower bound constraint

for the average speed. This problem has been tackled in a railway context by Văsak et al. (2009) who use dynamic programming to compute the optimal control of an electric train with a fixed arrival time constraint.
In this study, we propose to validate a design method of minimal energy control by comparing it to the exact solution in the case where it can be computed i.e. when all terms of the problem, including the slope of the road, are described by analytic expressions. The practical relevance of the study is based upon the fact that the model of the electric bicycle has been calibrated from experiments with a real device and that the validated approximate method can take into account digitized travel profiles available in Geographical Information Systems Taylor and Blewitt (2006). With this aim in mind, this paper is organized as follows.
In section 2, the structure of a generic model of an electric bicycle is presented and its parameters are calibrated. Considering an analytical road profile, an exact continuous time optimal control is first presented in section 3. It is based upon the Pontryaguin maximum principle and the computation is possible because the model, objectives and constraints are all given as analytical smooth functions. Section 4 presents a second method that can use punctual specifications of the road profile. It is based upon the A* algorithm with an appropriate heuristic function and the discretizing policy to implement it is defined. Finally, section 5 validates this second practical method by comparing its performances with those of the exact method on the same test bench.

2 MODEL DESCRIPTION

2.1 Mechanical model

The altitude profile $z(s)$ of the considered travel is presented on figure 1 where the position of the bicycle is termed by the curvilinear abscissa s. It shows downhill and uphill phases with variable lengths and slopes and it is described analytically by a C^∞ function.

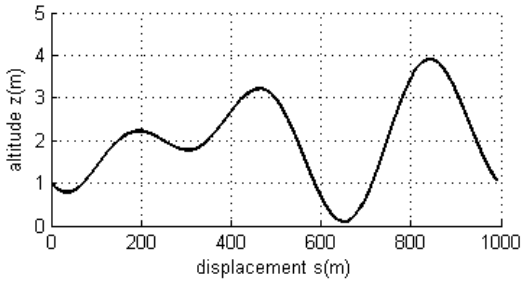

Figure 1: Altitude profile of the trip

For the sake of analytic simplicity and without loss of generality, we use in the sequel the angular position of the motor $x_1(t)$ in place of the curvilinear abscissa $s(t)$. The relation between these variables is: $s(t) = R_w x_1(t)$ where R_w denotes the radius of the wheel hub motor. Let us classically consider (1) as the state vector.

$$\vec{x}(t) = \begin{pmatrix} x_1(t) \\ x_2(t) \end{pmatrix} = \begin{pmatrix} x_1(t) \\ \dot{x_1}(t) \end{pmatrix} \tag{1}$$

The bicycle is only powered by the electric motor and is subject to the air drag, the rolling resistance of the tires and the gravity (Martin et al. (1998)). The wind speed is assumed to be null. The second Newton's law gives:

$$J\frac{dx_2}{dt} = T_m(u, x_2) + T_R + T_g(x_1) + \alpha.(x_2)^2 \tag{2}$$

where the terms are:

- $u(t)$: the control input which is the voltage of the electrical motor,
- $\alpha.(x_2)^2$: the torque induced by the air drag,
- $T_m(u, x_2)$: the torque of the electrical motor,
- $T_g(x_1)$: the torque induced by the slope,

$$T_g(x_1) = -mg\frac{dz}{dx_1}(x_1) \tag{3}$$

Table 1 sums up the parameters values of the experimental setup.

rolling resistance torque	T_R	$-1.9N.m$
air drag coefficient	α	$-0.02N.m.rad^{-2}.s^2$
equivalent inertia	J	$10kg.m^2$
mass (bicycle + cyclist)	m	$115kg$
gravity	g	$9.81m.s^{-2}$
wheel radius	R_w	$0.33m$

Table 1: Bicycle parameters

2.2 Electric model

The electric bicycle is powered by a synchronous motor. This kind of motor can be efficiently modeleled by a Direct Current motor model:

Torque of the motor:

$$T_m(t) = k_i\frac{u(t) - k_v x_2(t)}{R_c} + T_f \tag{4}$$

Electric power:

$$P_e(t) = u(t)\frac{u(t) - k_v x_2(t)}{R_c} \tag{5}$$

Mechanical power:

$$P_m(t) = T_m(t)x_2(t) \tag{6}$$

The parameters of the model have been identified by using a test bench depicted on figure 2.

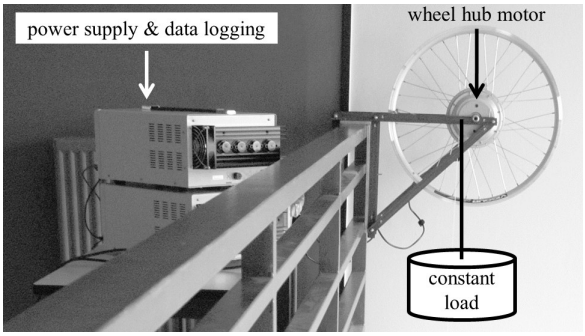

Figure 2: The motor test bench

In this experimental setup, the motor is loaded by a constant resistive torque. Angular velocity, voltage and current are measured simultaneously in order to compare the mechanical power output with the electrical power input.

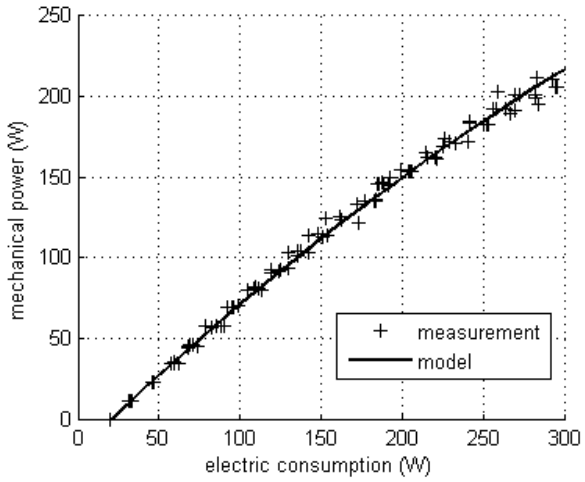

Figure 3: Calibration of the motor model

Current constant	k_i	$1.43.N.m.A^{-1}$
Speed constant	k_v	$1.5V.rad^{-1}.s$
Coil resistance	R_c	1Ω
Internal friction torque	T_f	$-0.7N.m$

Table 2: Bicycle parameters

Table 2 sums up the parameters value of the motor and figure 3 shows the relevance of the calibration. The parameters T_R and α have been calibrated by using an instrumented bicycle running down a slope with a non-pedaling cyclist. The result of the calibration of the bicycle model is displayed on figure 4.

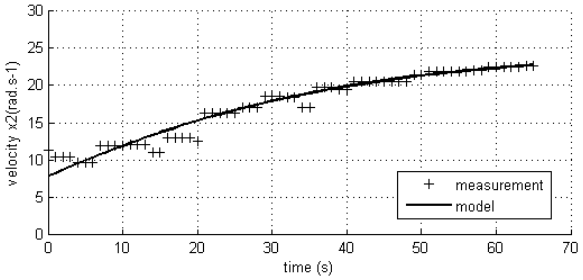

Figure 4: Calibration of the complete model

$T_0 = T_R + T_f$ denoting an equivalent friction torque, the state space model (7) sums up equations (2, 4).

$$\Phi \triangleq \begin{cases} \frac{dx_1}{dt} = x_2 \\ \frac{dx_2}{dt} = \frac{1}{J}\left[\frac{k_i}{R_c}u - \frac{k_i k_v}{R_c}x_2 + T_0 + \right. \\ \qquad \left. \alpha.(x_2)^2 + T_g(x_1)\right] \end{cases} \tag{7}$$

3 EXACT OPTIMAL CONTROL

3.1 Definition of the optimization problem

The energy consumption is defined as the integral of the power (5). Considering a constant efficiency of the battery gives the cost function to be minimized as:

$$E_e = \int_{t_0}^{t_f} P_e(t)dt = \int_{t_0}^{t_f} u(t)\frac{u(t) - k_v x_2(t)}{R_c}dt \tag{8}$$

The trip to be performed is specified by 1) a 3D path, 2) a given time interval $[t_0, t_f]$. According to the choice (1) of state variables, starting with a zero initial velocity is expressed as:

$$\begin{cases} x_1(t_0) = 0 \\ x_2(t_0) = 0 \end{cases} \tag{9}$$

The final time t_f is chosen but both final position $x_1(t_f)$ and speed $x_2(t_f)$ are free variables. In the sequel, a lower bound for the average velocity of the bicycle is chosen as 15km/h which corresponds to:

$$\bar{x}_2 = \frac{1}{t_f - t_0}\int_{t_0}^{t_f} x_2(t)dt \geq 12.5rad.s^{-1} \tag{10}$$

3.2 Necessary conditions for the optimal control

The exact design of an optimal control is achieved by maximizing, at any time, the Hamiltonian func-

tion (11) (Lewis and Syrmos (1995) and Pontryaguin (1974)).

$$H = -\frac{u^2}{R_c} + \frac{k_v}{R_c}x_2 u + \gamma x_2 + \lambda_1 x_2 + \lambda_2 \frac{1}{J}\left[\frac{k_i}{R_c}u - \frac{k_i k_v}{R_c}x_2 + T_0 + \alpha.(x_2)^2 + T_g(x_1)\right] \quad (11)$$

The term $-\frac{u^2}{R_c} + \frac{k_v}{R_c}x_2 u$ represents the opposite of the electric power. The maximisation of the Hamiltonien function leads to the minimization of the integral of the electric power along the path i.e. the minimisation of the cost function E_e (8). The term γx_2 tunes the average speed along the path (10). The co-state vector $\vec{\lambda}(t)$ may be thought a Lagrange parameter vector associated with the state equation (7) concidered as an equality constraint. The term $\lambda_1 x_2$ adresses the first line of the state equation and $\lambda_2 \frac{1}{J}\left[\frac{k_i}{R_c}u - \frac{k_i k_v}{R_c}x_2 + T_0 + \alpha.(x_2)^2 + T_g(x_1)\right]$ adresses the second one. Maximizing the Hamiltonian yields the necessary conditions (12, 13) on the co-state $\vec{\lambda}(t)$.

$$\Psi \triangleq \begin{cases} \frac{d\lambda_1}{dt} & = -\frac{\partial H}{\partial x_1} \\ \frac{d\lambda_2}{dt} & = -\frac{\partial H}{\partial x_2} \end{cases}$$

$$\frac{d\lambda_1}{dt} = -\frac{1}{J}\lambda_2 \frac{\partial T_g}{\partial x_1} \quad (12)$$

$$\frac{d\lambda_2}{dt} = -\frac{k_v}{R_c}u - \gamma - \lambda_1 + \lambda_2 \frac{1}{J}\left(\frac{k_i k_v}{R_c} - 2\alpha x_2\right) \quad (13)$$

The control $u(t)$ maximizes the Hamiltonian. This implies the relation (14) in the interior of its definition domain, e.g. when it does not saturate.

$$\frac{\partial H}{\partial u} = -\frac{2}{R_c}u + \frac{k_v}{R_c}x_2 + \frac{k_i}{JR_c}\lambda_2 = 0 \quad (14)$$

Taking into account the saturation, equation (14) leads to the exact optimal control:

$$u = sat\left(\frac{k_v}{2}u + \frac{k_v}{2J}\lambda_2\right) \quad (15)$$

3.3 Implementation of the optimal control

Differential relations governing the state (7) and the co-state (12, 13) are nonlinear, strongly coupled and must thus be integrated in parallel. Although Van Keulen et al. (2011) and Kim et al. (2011) present different methods to compute analytically the co-state by using a simplified model, we prefer to integrate the non-simplified one with a numerical integration method whose main lines is described by the Matlab Simulink® block-diagram (figure 5). This implies the knowledge of the initial values of both state and co-state. The former is a priori given (9) but the later must be estimated.

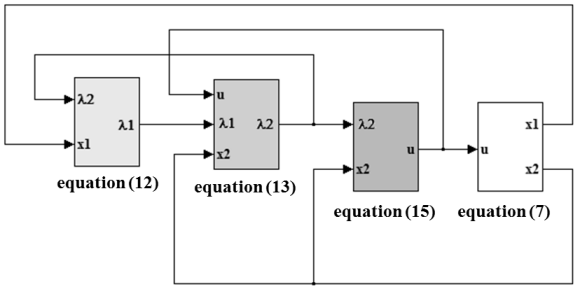

Figure 5: Computing the control. Block-diagram describing the simultaneous integration of the state and co-state. Each block is designed to compute a specific variable.

3.4 Defining the co-state initial conditions

The state space of the optimal process (state + co-state, figure 5) is 4 dimensional but only 2 initial conditions are a priori given (9) and the initial value $\vec{\lambda}(t_0)$ of the co-state and the Lagrange's parameter γ remain to be determined. A first simplification stems from a change of variables. Considering (12, 13), we merge γ and $\lambda_1(t)$ into a new variable: $\lambda_1'(t) = \gamma + \lambda_1(t)$. Since γ is a constant, the time derivative of $\lambda_1'(t)$ is the same as the one of $\lambda_1(t)$. The search for initial conditions is now restricted to only 2 parameters, $(\lambda_1'(t_0), \lambda_2(t_0))$ instead of the 3 original ones, $(\gamma, \lambda_1(t_0), \lambda_2(t_0))$. Delprat et al. (2004) solve a similar problem with only one boundary condition by using a bisection search, making profit of the monotonicity of the cost function.

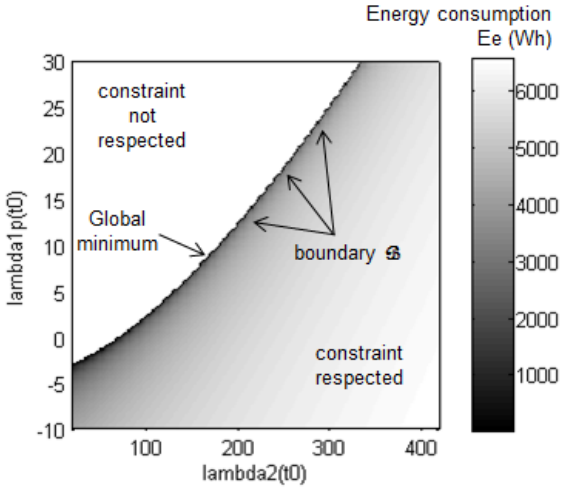

Figure 6: Energy consumption mapping

To get an insight of the 2 parameters search in the present case, consider figure 6 where the $(\lambda_1'(t_0), \lambda_2(t_0))$ plane is split in 2 regions: 1) a non-admissible one, where the average speed constraint (10) is not fulfilled and 2) an admissible one, where the value of the cost function $E_e(\lambda_1'(t_0), \lambda_2(t_0))$ is computed and displayed in grayscale. The limit between the two zones is described by a boundary curve B where the constraint is saturated. Examine the cost function along the boundary curve B on figure 7, it appears as a convex function. The global minimum can then found by using a 2 steps algorithm using bisection.

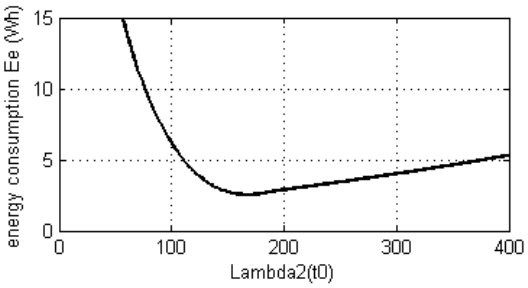

Figure 7: Energy consumption mapping

3.5 Performance of the optimal control

$(\lambda_1'(t_0), \lambda_2(t_0))$ being known, the optimal control is obtained by integrating the process of figure 5. We propose here to illustrate the benefit gained from the optimal control by comparing it to a constant control (16) that satisfies the same limit conditions and saturates the average speed constraint.

$$\begin{cases} \forall t,\ u(t) = u_c \\ \\ \bar{x_2} = 12.5 rad.s^{-1} \end{cases} \tag{16}$$

Results are displayed on figure 8. The optimal control saves 10.5% of energy with respect to the constant control policy. In particular, let us notice that the optimal control uses regenerative breaking to convert kinetic energy into electric energy at the end of the trip. Van Keulen et al. (2011) report a similar behaviour.
These results need a twice differentiable analytical altitude profile whereas the experimental data are just sequences of points. This motivates the interest for the discrete approach detailed in the next section.

4 A* SUBOPTIMAL CONTROL ALGORITHM

In robotics, optimal control is often used for path planning among obstacles Latombe (1991) and LaValle (2006). The practical way to compute the solution often consists to discretize the problem before

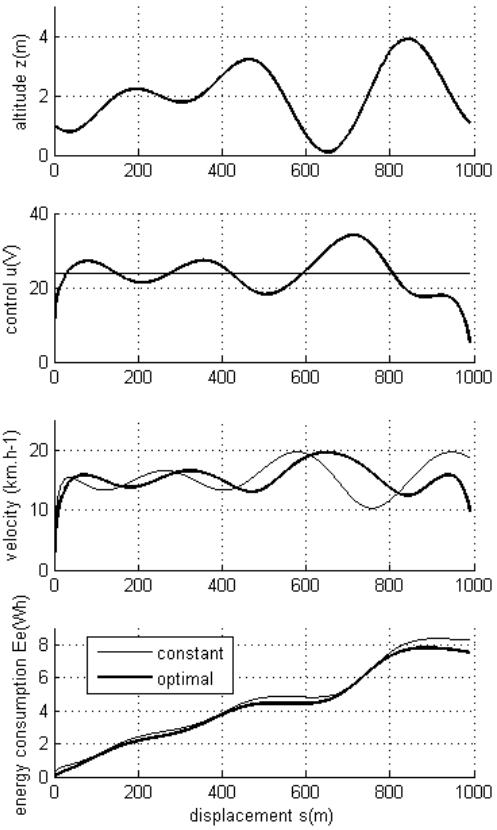

Figure 8: Comparison of performances between constant control and optimal control

applying an optimal graph search technique. It begins by sampling the time, the control and the state space Thrun et al. (2005).

4.1 sampling time and state

Fist, the time is uniformly sampled with a period Δt.

$$\begin{aligned} &k \in \left\{0; ...; k_f = ceil\left(\tfrac{t_f - t_0}{\Delta t}\right)\right\} \\ &t_k = t_0 + k\Delta t \end{aligned} \tag{17}$$

Second, the state variables are too uniformly sampled.

$$\vec{x}_k = \begin{cases} x_{1,k} \in \{0; \Delta x_1; ...; x_1^{max}\} \\ \\ x_{2,k} \in \{0; \Delta x_2; ...; x_2^{max}\} \end{cases} \tag{18}$$

At each time sample t_k the computed continuous state $\vec{x}(t_k)$ is rounded to the nearest discrete state $\vec{x}_k$. The maximum available velocity depends on the maximum control and the altitude profile. The rotary speed is upper bounded by $x_2^{max} = 25 rad.s^{-1}$ which correspond to a $29.7 km.h^{-1}$ velocity. The maximum available position is $x_1^{max} = x_2^{max} t_f$. Aliasing errors on both position and velocity occur due to the quantization. For coherence sake, sampling space periods $(\Delta x_1, \Delta x_2)$ are chosen so that $\Delta x_1 = \Delta x_2 \Delta t$.

4.2 Sampling the control

Optimal energy controls are continuous ones whereas a discrete control strategy chooses inside a finite set at each time sample. We thus propose to define the control signal as a continuous piecewise affine function (figure 9).

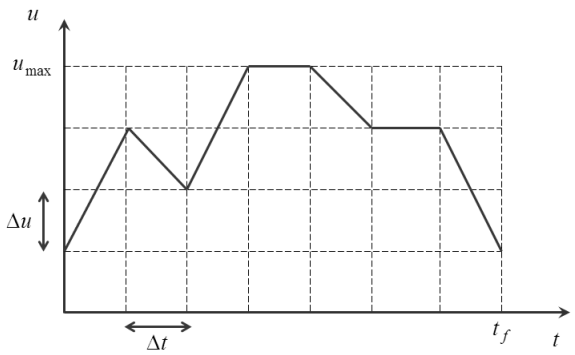

Figure 9: Example of the continuous piecewise affine function $u(t)$

At any time t_k, a value of the control u_{k+1} is chosen among a uniformly sampled set of controls.

$$u_{k+1} \in \{0; \Delta u; ...; u_{max}\} \tag{19}$$

The saturation of the control is given by the voltage of the battery $u_{max} = 40V$. The continuous control function $u(t)$ (20) is defined from the elements of the list $\{u_0, u_1, ..., u_f\}$ by a piecewise affine function.

$$\begin{aligned} &k \in \{0; 1; ...; k_f - 1\} \\ &u(t) = u_k + \tfrac{u_{k+1}-u_k}{\Delta t}(t - t_k) \quad t \in [t_k, t_{k+1}] \end{aligned} \tag{20}$$

4.3 Rewriting of the optimal control problem

The optimal control problem consists now to compute the sequence $\{u_0; u_1; ...; u_f\}$ that minimizes the cost function E_e while satisfying the average speed constraint (10). At each sampled state $\vec{x}_k$, the new sampled control u_{k+1} is chosen and the state evolution during the time interval $[t_k, t_{k+1}]$ is computed by first, integrating the state equation (7) submitted to the control (20) and then rounding into the new discrete state $\vec{x}_{k+1}$. The state evolution is thus described by a graph where the states $\vec{x}_k$ are the nodes and each admissible control defines a link (figure 10). This graph is dynamically built.
The valuation of the links between $\vec{x}_k$ and $\vec{x}_{k+1}$ is the energy consumption between t_k and t_{k+1}.
The optimal control problem consists now in finding the minimal cost path in the graph between the initial state and the final domain.
From a complexity point of view, note in (21) that the number of a priori available paths n_{av} increases drastically when refining the quanta Δu and Δt.

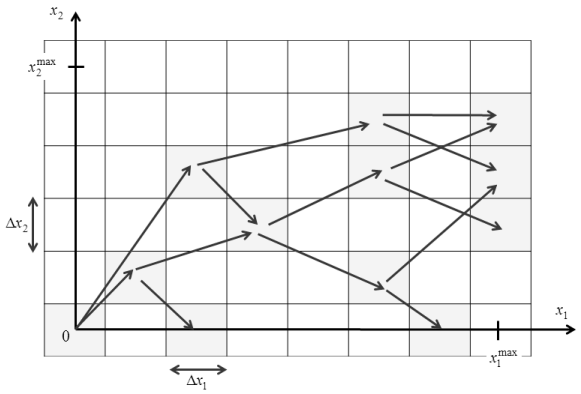

Figure 10: Example of a sampled space state with different available paths. The gray squares represent the nodes, the arrows represent the links.

$$n_{av} = \left(\frac{u_{max}}{\Delta u} + 1\right)^{\left(\frac{t_f}{\Delta t}+1\right)} \tag{21}$$

4.4 Optimal pathfinding using A* algorithm

The Dijkstra's Algorithm solves optimal pathfinding problems in graphs with a breadth first search strategy which implies the exploration of all possible paths with the consequence of huge computation times.
The A* algorithm (Dechter and Pearl (1985)) is based on Dijkstra's method but it explores first the most promising path. The keypoint to qualify a promising path consists to compute an estimate of the optimal valuation for each examined node. This criterion is the sum of current criterion associated with the path from the beginning to the current node plus a heuristic guess $h(\vec{x}_k)$ of the part of the criterion associated with remaining path to the goal.
Usually, this directed depth first search strategy shortens the computation time. The definition of the heuristic $h(\vec{x}_k)$ is the keystone of the computational efficiency. This heuristic must be designed according to contradictory guidelines: 1) it must be a lower bound of the energy left to spend from the current to the final nodes and 2) the more the heuristic is accurate the faster the algorithm will converge.
The heuristic presented here is based on a balance between the work of mechanical loss (friction and air drag) and the available mechanical energies (kinetic and potential). The work of friction resistance W_r is given by:

$$W_r = \int_{t_k}^{t_f} T_0 x_2(t) dt = T_0(x_{1,f} - x_{1,k}) \tag{22}$$

The work of the air drag W_a is upper bounded by:

$$W_a = \int_{t_k}^{t_f} \alpha \left[x_2(t)\right]^3 dt \leq \alpha \frac{(x_{1,f} - x_{1,k})^3}{(t_f - t_k)^2} = W_a^{max} \quad (23)$$

Notice that both mechanical works W_r and W_a are negative. The kinetic energy is a mechanical available energy given by the expression:

$$T = \frac{1}{2} J (x_{2,k})^2 \quad (24)$$

The potential energy of gravity U_g is deduced from the sampled altitude profile $z(x_{1,k}) = z_k$.

$$U_g = \int_{t_k}^{t_f} T_g(x_1) x_2(t) dt = mg(z_k - z_f) \quad (25)$$

To link the mechanical energy with the cost function, we use the motor efficiency defined by:

$$\eta(u, x_2) = \frac{P_m(u, x_2)}{P_e(u, x_2)} \quad (26)$$

The expression (26) can be upper bounded by a constant:

$$\eta_{max} = \max_{u, x_2} \left[\eta(u, x_2)\right] \leq \frac{k_i}{k_v} \quad (27)$$

Considering (22), (23), (24), (25) and (27), the heuristic is defined:

$$h = \frac{k_v}{k_i} \left(-W_r - W_a^{max} - U_g - T\right) \quad (28)$$

4.5 RESULTS

To compare the exact optimal control and the A* algorithm, four different simulations have been performed with different travelled distance: 250m, 500m, 750m and 1000m. The A* algorithm needs a sampling strategy in order to compute in reasonable time a near optimal solution. Good results have been obtained with a control quantum $\Delta u = 4V$ and a speed quantum $\Delta x_2 = 0.5 rad.s^{-1}$. The time period Δt is a tuning parameter. It has been reduced regularly in order to check if the computation converges. The energy curve reaches an asymptot for a computation time that does not exceed 300s (figure 11).

The shape of the control obtained by the A* algorithm converge to a piecewise affine function that fits the optimal one in every case (figures 12 to 15). The performances of energy minimization are compared in table 3. The relative difference of performance between A* algorithm and optimal control is mainly 1.2% and does not exceed 1.35%.

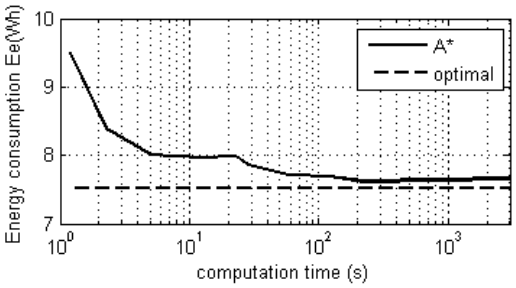

Figure 11: Convergence of the A* compared with the optimal reference

The A* algorithm converges to a solution that is sub optimal, with a much shorter computation time (table 4). The benefit of using the proposed heuristic (28) is evident when one considers the computation time of a Dijkstra's algorithm exploring all available links. Its computation time can be estimated with the computation time of a link (0.5 ms) multiplied by the number of links available (21).

The computation time of the A* algorithm strongly depends of the heuristic function accuracy. The presented heuristic function neglects a huge number of links in order to explore only the more promising. For example, among a $n_{av} \approx 3.45 * 10^{13}$ maximum number of links, the A* algorithm only explores $n_{ex} \approx 3.48 * 10^5$ ones.

On the energy consumption curves (figures 12 to 15) the heuristic is also depicted. Notice for example that in figure 15 at the begining of the trip, the heuristic estimated the energy left to spend at $h(\vec{x}_0) = 5Wh$. To verify this estimation notice that the real energy consumed at the end of the trip is $E_e(\vec{x}_f) = 7.53Wh$. The relative difference is about 33%. This good accuracy of the heuristic function explains such good performances in terms of computation time.

distance (m)	optimal (Wh)	A* (Wh)	relative difference
250	2.54	2.56	1.10 %
500	4.54	4.59	1.27 %
750	5.64	5.78	1.35 %
1000	7.53	7.62	1.07 %

Table 3: Comparison of the energy consumption

5 CONCLUSION AND PERSPECTIVES

In this communication, a practical minimal energy control computation has been validated with respect

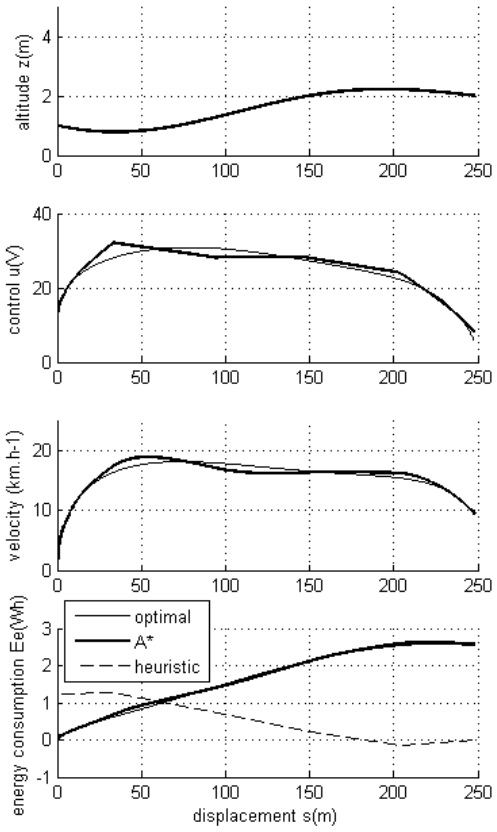

Figure 12: Comparison between optimal control and A* algorithm for a travelled distance of 250m.

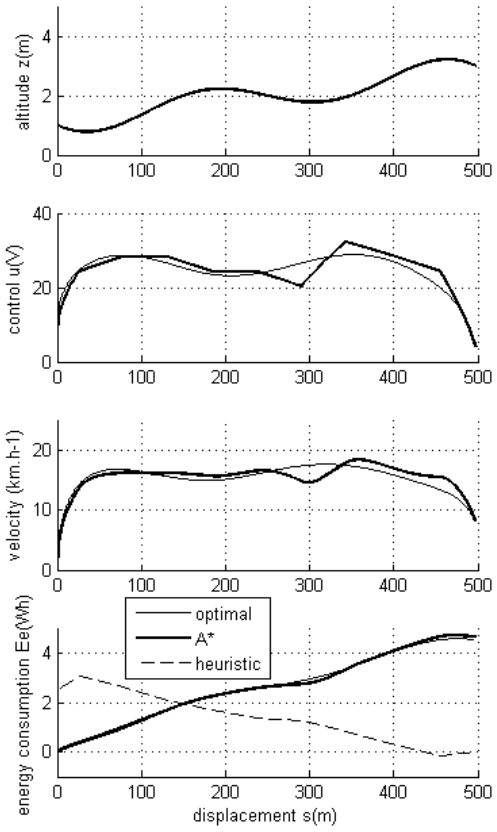

Figure 13: Comparison between optimal control and A* algorithm for a travelled distance of 500m.

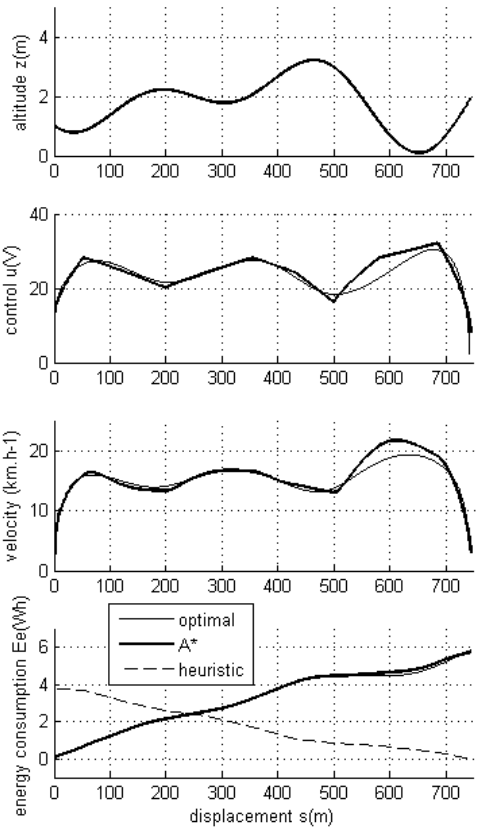

Figure 14: Comparison between optimal control and A* algorithm for a travelled distance of 750m.

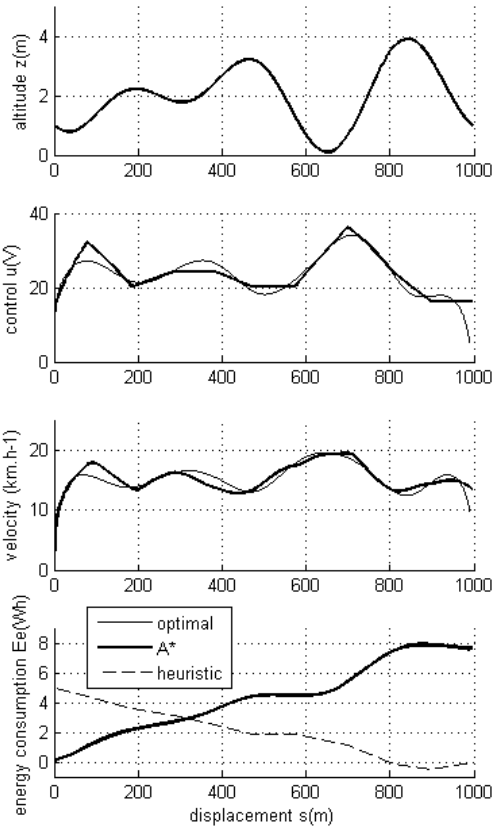

Figure 15: Comparison between optimal control and A* algorithm for a travelled distance of 1000m.

distance (m)	optimal (s)	A* (s)	Dijkstra's estimation
250	786	4	886 s
500	1212	42	547 years
750	1590	53	547 years
1000	1784	312	547 years

Table 4: Comparison of computation times, optimal algorithm and A* are measured, Dijkstra's one is estimated

to a single energy electric bicycle. The main originality of the method is the definition of the heuristic cost function used by the A* algorithm that performs the search of the optimal path in the discretized search space. The validation has been obtained by comparing the results of the proposed algorithm with those of the exact solution when they are both applied to an academic realistic case.
The relevance of the method to practical cases stems from the fact that 1) it can use digital maps to compute optimal paths, 2) the computation time is reasonable and 3) the process model has been calibrated with real data.
The incoming studies will face the energy hybridization problem by using more realistic models of the electrical bicycle including the behaviour of the cyclist proposed by Grossoleil and Meizel (2010). The dynamic model of the battery proposed by Tremblay and Dessaint (2009) could be interesting to build a more realistic cost function. Finally, optimizations applied at long travels with a profile of altitude measured in real conditions will be performed with the validated A* Algorithm.

REFERENCES

R. Dechter and J. Pearl. Generalized best-first search strategies and the optimality of A*. *J. ACM*, 32 (3):505–536, July 1985.

S. Delprat, J. Lauber, T.M. Guerra, and J. Rimaux. Control of a parallel hybrid powertrain: Optimal control. *IEEE Transactions on Vehicular Technology*, 53(3):872–881, may 2004.

D. Grossoleil and D. Meizel. Modelling the hybridisation of human and artificial energy applied at an electrical bicycle. volume 11, pages 416–421, 2010.

T.S. Kim, C. Manzie, and R. Sharma. Two stage optimal control of a parallel hybrid vehicle with trafic preview. 2011.

J.C. Latombe. *Robot motion planning*. Springer, 1991.

S.M. LaValle. *Planning Algorithms*. Cambridge University Press, may 2006.

F.L. Lewis and V.L. Syrmos. *Optimal control second edition*. Wiley Interscience, 1995.

C.C. Lin, H. Peng, J.W. Grizzle, and J.M. Kang. Power management strategy for a parallel hybrid electric truck. *IEEE Transactions on Control Systems Technology*, 11(6):839–849, 2003.

J.C. Martin, D.L. Milliken, J.E. Cobb, K.L. McFadden, and A.R. Coggan. Validation of a mathematical model for road cycling power. *Journal of Applied Biomechanics*, 14(3):276–291, 1998.

L.S. Pontryaguin. *Théorie Mathématique des Processus Optimaux*. Edition MIR, Moscou, 1974.

G. Taylor and G. Blewitt. *Intelligent Positioning. GIS-GPS unification*. J. Wiley, Chichester, 2006.

S. Thrun, W. Burgard, and D. Fox. *Probabilistic robotics*. MIT Press, 2005.

J.M. Timmermans, J. Matheys, P. Lataire, J. Van Mierlo, and J. Cappelle. A comparative study of 12 electrically assisted bicycles. *World Electric Vehicle Journal*, 3, 2009.

O. Tremblay and L.A. Dessaint. Experimental validation of a battery dynamic model for ev applications. *World Electric Vehicle Journal*, 3, 2009.

T. Van Keulen, B. de Jager, and M. Steinbuch. Optimal trajectories for vehicles with energy recovery options. *18th IFAC World Congress Milano*, 2011.

M. Văsak, M. Baotić, N. Perić, and Bago M. Optimal rail route energy management under constraints and fixed arrival time. *Proceedings of the European Control Conference*, 2009.